catalysts

MDPI

Article

Inhibiting Fe–Al Spinel Formation on a Narrowed Mesopore-Sized $MgAl_2O_4$ Support as a Novel Catalyst for H_2 Production in Chemical Looping Technology

Ali Hafizi and Mohammad Reza Rahimpour *

Department of Chemical Engineering, Shiraz University, Shiraz 71345, Iran; hafizi@shirazu.ac.ir
* Correspondence: rahimpor@shirazu.ac.ir

Received: 13 October 2017; Accepted: 29 December 2017; Published: 15 January 2018

Abstract: In this paper, the structure of Al_2O_3 is modified with magnesium to synthesize $MgAl_2O_4$ as an oxygen carrier (OC) support. The surface properties and structural stability of the modified support are improved by the incorporation of magnesium in the structure of the support and additionally by narrowing the pore size distribution (about 2.3 nm). Then, iron oxide is impregnated on both an Al_2O_3 support and a $MgAl_2O_4$ support as the oxygen transfer active site. The XRD results showed the formation of solely Fe_2O_3 on the $MgAl_2O_4$ support, while both Fe_2O_3 and Fe_3O_4 are detected in the synthesized Fe_2O_3-Al_2O_3 structure. The synthesized samples are investigated in chemical looping cycles, including CO reduction (as one of the most important side reactions of chemical looping reforming), at different temperatures (300–500 °C) and oxidation with steam at 700 °C for hydrogen production. The obtained results showed the inhibition of Fe–Al spinel formation in the structure of the Fe_2O_3-$MgAl_2O_4$ OC. In addition, H_2 with a purity higher than 98% is achievable in oxidation of the OC with steam. In addition, the activity and crystalline change of the Fe_2O_3-$MgAl_2O_4$ OC is investigated after 20 reduction-oxidation cycles.

Keywords: chemical looping; oxygen carrier; hydrogen production; narrow pore size distribution; Fe_2O_3 dispersion; texture modification

1. Introduction

The production of hydrogen (as an energy carrier) from primary resources, such as methane and water, is industrially developed [1–4]. Hydrogen with high purity can be applied in different applications, such as fuel cells. Nevertheless, most hydrogen production processes need further purification with the purpose of preventing electrode poisoning [5]. One-step pure hydrogen production has attracted attention during the past few years [6,7]. The chemical looping technique (CLT) is known as a novel process for hydrogen production from different sources. Chemical looping processes are based on the transportation of lattice oxygen from an oxidizing solid environment to a reducing environment in two interconnected reactors called the "fuel reactor" and the "oxidation reactor" as indicated in Figure 1 [8,9]. The principal reactions involved in the chemical looping steam methane reforming (CL-SMR) process are as follows [10,11]:

Fuel reactor:

$$CH_4 + Me_xO_y \rightarrow CO + 2H_2 + Me_xO_{y-1} \quad (1)$$

Oxidation reactor:

$$H_2O + Me_xO_{y-1} \rightarrow H_2 + Me_xO_y \quad (2)$$

The in-situ oxidation of carbon monoxide is one of the most important side reactions to progress the reaction network toward pure hydrogen. Carbon monoxide can be used as a reducing agent and the steam is used as an oxidant as indicated in the following reactions:

$$CO + Me_xO_y \rightarrow CO_2 + Me_xO_{y-1} \quad (3)$$

Therefore, hydrogen with high purity could be obtained in both the oxidation and reduction periods of chemical looping cycles, which is depicted in Figure 1.

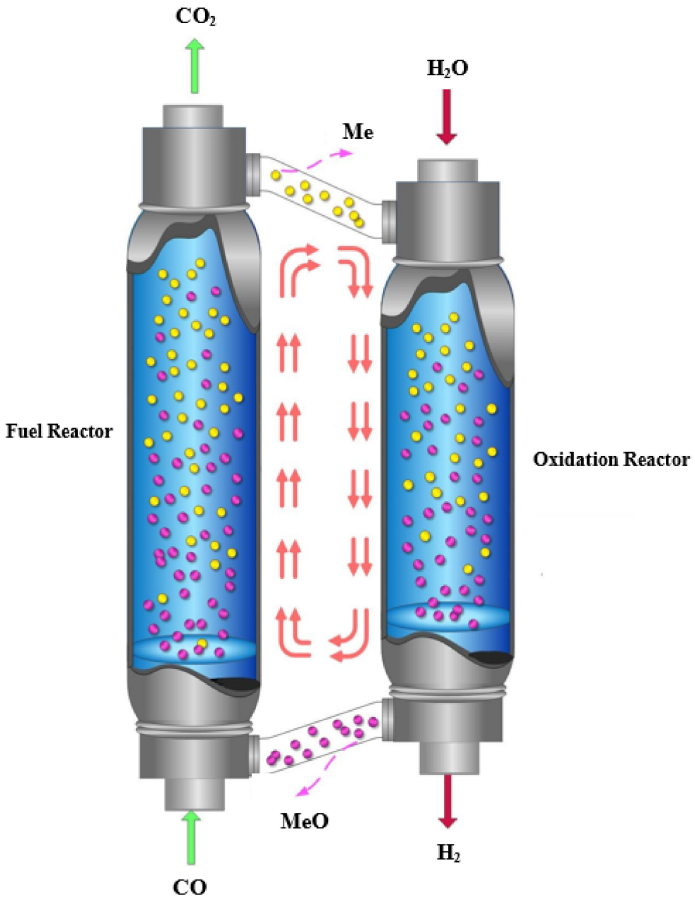

Figure 1. Conceptual scheme of chemical looping reforming technology.

The selection of an appropriate oxygen carrier (OC) has a significant impact on the reaction performance of this process. Recently, the application of metal oxides as oxygen transfer media have attracted much attention [11–13]. The lattice oxygen released from these composites has the advantage of being pure in addition to transferring lattice oxygen intelligently. The selection of a suitable OC seems to be of great importance in large-scale use. The oxygen carrier must have sufficient oxygen transport capacity, high reactivity, easy oxygen release, sorption properties, agglomeration resistance, a low cost, no environmental impact, and high chemical and mechanical stability [14,15]. One of the major challenges in the large-scale usage of oxygen transfer materials is the development of a stable OC in continuous alternating cycles of reduction and oxidation without deactivation. Fe_2O_3 is known as one of the best candidates among different metal oxides because of its low cost, high thermal resistance, and its thermodynamic tendency toward H_2 production [11]. In an iron-based OC, the oxygen is mainly supplied from the reduction of hematite to magnetite ($Fe_2O_3 \rightarrow Fe_3O_4 \rightarrow Fe_{0.947}O$) in the presence of oxygen demandant for the first cycle. The first step of the reaction occurs faster than other iron oxide reduction reactions. The reoxidation reaction ($Fe_{0.947}O + H_2O \rightarrow H_2 + Fe_3O_4$) occurs by passing steam

over the OC bed at high temperatures in order to regenerate the reacted OC. The oxidation of the reduced oxygen carrier ($Fe_{0.947}O$) with steam for the production of hydrogen is thermodynamically limited. Thus, magnetite (Fe_3O_4) could be formed after oxidization with steam [16,17].

The active metal oxide should be supported on an appropriate material that can effectively increase the surface area and availability of active metal oxides, improves the OC's structural properties, and subsequently increases its reactivity [18]. Al_2O_3 is known as one of the best catalysts and oxygen carrier supports owing to its high stability (chemical and mechanical) and considerably higher melting temperature [18]. However, the imperfect formation of iron-alumina spinel ($FeAl_2O_4$) is an important phenomenon that occurs at high temperatures. Furthermore, the transformation of primary formed iron oxide particles to Fe_3O_4 on the support surface is the other defect of aluminum oxide as the OC support [11]. The formation of $FeAl_2O_4$ in the OC structure could deactivate the iron oxides and slow down the rate and capacity of oxygen transference.

Despite these well-known problems, many efforts have been made to enhance the activity and stability of an iron-based oxygen carrier. There are several ways currently being applied to reach this purpose, such as applying various types of supports with enhanced structural and textural properties [19–21], and the application of different promoters and inhibitors are the most important efforts to solve these drawbacks [22–27].

With the purpose of suppressing the carbon deposition and improving its catalytic activity, a wide diversity of promoters, such as lanthanum, cerium, magnesium, and calcium, have been incorporated into the structure of the support [28–30]. Li et al. [28] assessed ceria-promoted Ni/SBA-15 catalysts for ethanol steam reforming. The results showed that the incorporation of CeO_2 could effectively control the size of Ni particles via strong metal–support interaction. Hafizi et al. [11] examined a Ca-promoted Fe/Al_2O_3 oxygen carrier in the chemical looping reforming of methane during the redox cycles. The obtained results showed the interaction of the calcium promoter and the alumina support for the improvement of an iron-based oxygen carrier with an inhibition of coke deposition. Ce-SBA-15-supported nickel catalysts were synthesized by Wang et al. [31] and applied for the dry reforming of methane. The results revealed that the cerium incorporated into the skeleton of the SBA-15 promoted the dispersion of nano-sized Ni particles and prohibited carbon formation.

The addition of magnesium to Al_2O_3 could effectively prevent the formation of Fe–Al spinel and improve the stability of the support at higher reaction temperatures by forming $MgAl_2O_4$ [8,31]. Furthermore, a rearrangement of the support's crystalline structure and a regulation of its pore size in a narrow distribution range with magnesium addition could effectively increase the OC's activity and stability. On the other hand, it could effectively control the coke deposition during reforming processes due to the nature of the Mg promoter.

This study investigates the effect of alumina and Mg–Al spinel as the support for the formation of Fe_2O_3. In addition, a narrowing of the oxygen carrier's pore size in the range of 2–3 nm is expected in order to control the coke deposition. The activity and feasibility of synthesized OC in the chemical looping process, including CO oxidation and hydrogen production in alternating cycles, were investigated at different temperatures. The crystalline phase transformation in the reduction-oxidation process is examined on the successfully synthesized Fe_2O_3-$MgAl_2O_4$ as an ultra-pure lattice oxygen transport medium.

2. Results and Discussion

2.1. Sample Characterization

The XRD patterns of Al_2O_3, Fe_2O_3-Al_2O_3, and Fe_2O_3-$MgAl_2O_4$ are shown in Figure 2a. The patterns were identified by the typical peaks of iron oxides, alumina, magnesium oxide, and spinel phases considering the JCPDS data bank. The XRD results suggest that the $MgAl_2O_4$ support could help the formation of pure Fe_2O_3, while alumina disperses iron on its surface in both the Fe^{2+} and Fe^{3+} forms.

The Fe_2O_3 could be clearly assigned at 2θ = 24.3°, 33.4°, 35.8°, 49.7°, 62.7°, 64.3°, and 89° in the XRD patterns of Fe_2O_3-Al_2O_3 and Fe_2O_3-$MgAl_2O_4$ according to JCPDS No. 01-084-0308. The formation of $MgAl_2O_4$ spinel is clear in the Mg-modified OC, and significantly inhibits the formation of iron alumina spinel. The diffraction peak at 37.6° for the (110) plane, 46° for the (111) plane, and 66.4° for the (211) plane of Al_2O_3 shifts about 0.4–0.8° to left in the Mg-promoted OC, representing the presence of $MgAl_2O_4$ spinel (JCPDS No. 01-073-2210) shown in Figure 2a. The four peaks located at 19.25°, 36.9°, 42.5°, and 66.3° match well with $MgAl_2O_4$. Furthermore, Mg or MgO species are not detected in the modified OC, which suggests the complete transformation of Mg to its spinel form. The XRD pattern of Fe_2O_3-$MgAl_2O_4$ after 20 reduction-oxidation cycles showed no iron–alumina spinel ($FeAl_2O_4$) formation (Figure 2b) at high reaction temperatures during the process (JCPDS No. 01-086-2320). However, our previous study on Fe_2O_3-Al_2O_3 or Fe_2O_3-CaO-Al_2O_3 oxygen transfer materials showed the formation of $FeAl_2O_4$ or $CaFe_2O_4$ in the OC structure after using it in the chemical looping process [11].

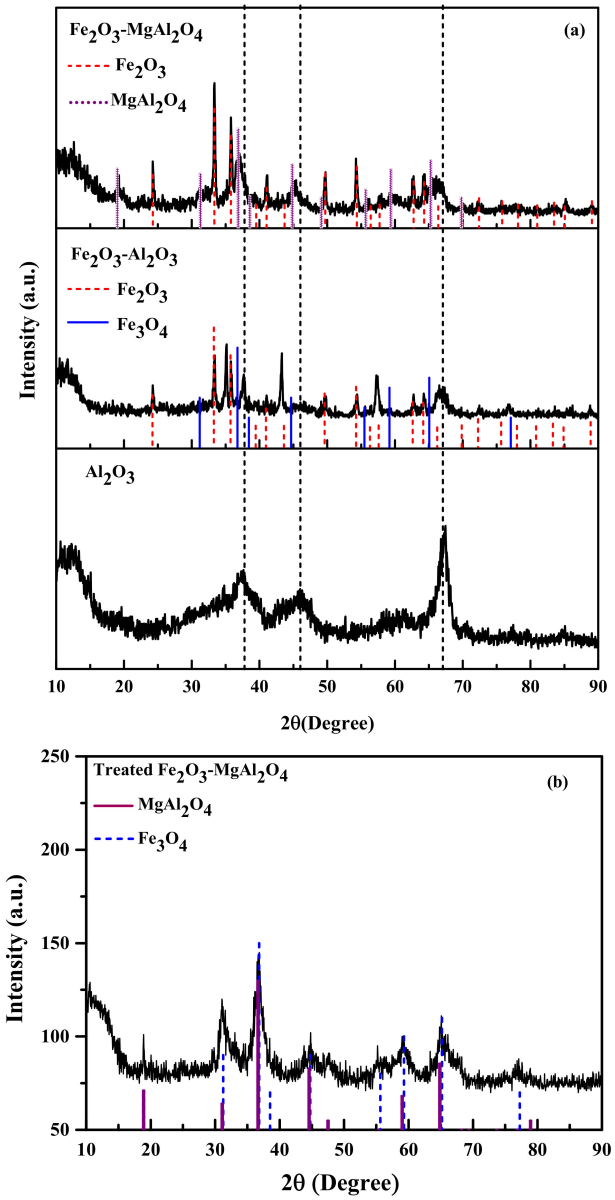

Figure 2. XRD patterns of (**a**) Al_2O_3, Fe_2O_3-Al_2O_3, and Fe_2O_3-$MgAl_2O_4$; (**b**) treated Fe_2O_3-$MgAl_2O_4$ in 20 redox cycles analyzed after the oxidation reaction.

Table 1 presents the physical properties, including Brunauer–Emmett–Teller (BET) surface area, pore volume average, pore size distribution, and energy dispersive X-ray Spectroscopy (EDX) results, of the synthesized OC samples. The BET surface area of the Fe_2O_3-Al_2O_3 is 174.3 m^2 g^{-1}, while the surface area of the Fe_2O_3-$MgAl_2O_4$ oxygen carrier shows a reduction to 113.1 m^2 g^{-1}. This reduction is due to the change of alumina structure and sequential calcinations that can result in pore blockage, sintering, and structural destruction. The reduction in pore volume from 0.416 to 0.389 cm^3 g r^{-1} can verify the reduction in surface area of the Mg-modified sample.

Table 1. Structural properties of the fresh and used samples.

Sample	Fe [a] (wt %)	Mg [a] (wt %)	Al [a] (wt %)	C [a] (wt %)	O [a] (wt %)	BET Surface Area (m^2 g^{-1})	Average Pore Size (nm)	Pore Volume (cm^3 g^{-1})
Fresh Fe_2O_3-Al_2O_3	17.72	-	39.82	-	42.46	174.3	4.3	0.416
Fresh Fe_2O_3-$MgAl_2O_4$	16.42	10.81	21.94	-	50.83	113.1	2.3	0.389
Used Fe_2O_3-Al_2O_3	16.97	-	40.01	5.83	37.29	-	-	-
Used Fe_2O_3-$MgAl_2O_4$	14.86	9.25	33.46	1.20	41.23	-	-	-

[a] Measured by EDX. BET: Brunauer–Emmett–Teller.

Figure 3 shows the Barrett–Joyner–Halenda (BJH) pore size distribution of both the Fe_2O_3-Al_2O_3 and Fe_2O_3-$MgAl_2O_4$ oxygen carriers. Since the average pore size distribution of the Fe_2O_3-Al_2O_3 is 4.3 nm, the distribution peak shows a wide range of pores (about 2–20 nm). On the other hand, the sharp peak of the Fe_2O_3-$MgAl_2O_4$ indicated in this figure confirms a narrow pore size distribution centered at 2.3 nm. Consequently, modifying the OC alumina support by Mg could effectively regulate the pore size distribution in a narrow range.

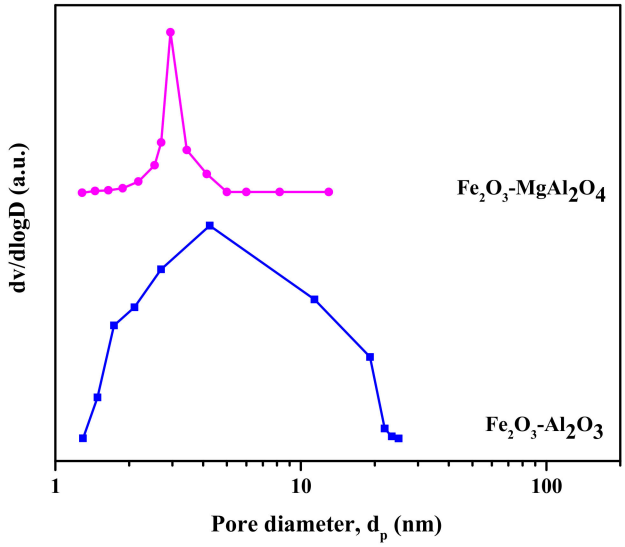

Figure 3. Pore size distributions of Fe_2O_3-Al_2O_3 and Fe_2O_3-$MgAl_2O_4$.

Field emission scanning electron microscopy (FESEM) micrographs of the prepared Al_2O_3, Fe_2O_3-Al_2O_3, and Fe_2O_3-$MgAl_2O_4$ samples are presented in Figure 4a–c. The synthesized blank alumina has a uniform aggregated surface as indicated in Figure 4a, and the distribution of Fe_2O_3-Al_2O_3 particles is indicated in Figure 4b. On the other hand, the Fe_2O_3-$MgAl_2O_4$ OC has approximately uniformly dispersed aggregated Fe_2O_3 particles (Figure 4c). A comparison of the FESEM graphs of both OC samples indicates that the structure of the Fe_2O_3-Al_2O_3 seems to have higher porosity than that of the Fe_2O_3-$MgAl_2O_4$. The FESEM-EDX results of the used Fe_2O_3-$MgAl_2O_4$

OC shown in Figure 4d and Table 1 revealed coke deposition of about 1.2 wt %. In addition, the slight aggregation of OC nanoparticles that is demonstrated in this figure could be due to the high oxidation temperature. The TEM image of the prepared Fe_2O_3-$MgAl_2O_4$ OC is shown in Figure 4e to examine the dispersion and size of iron oxide particles on the surface of the Mg–Al spinel. Nevertheless, the image shows the agglomeration of iron oxide particles with a diameter range of about 40–50 nm.

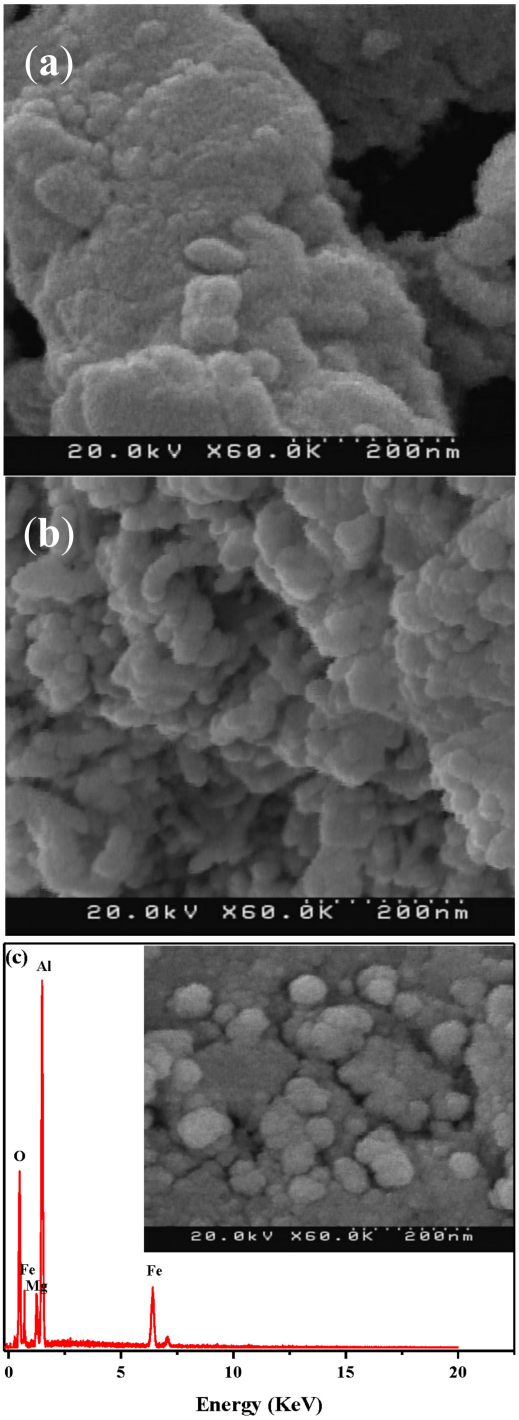

Figure 4. *Cont.*

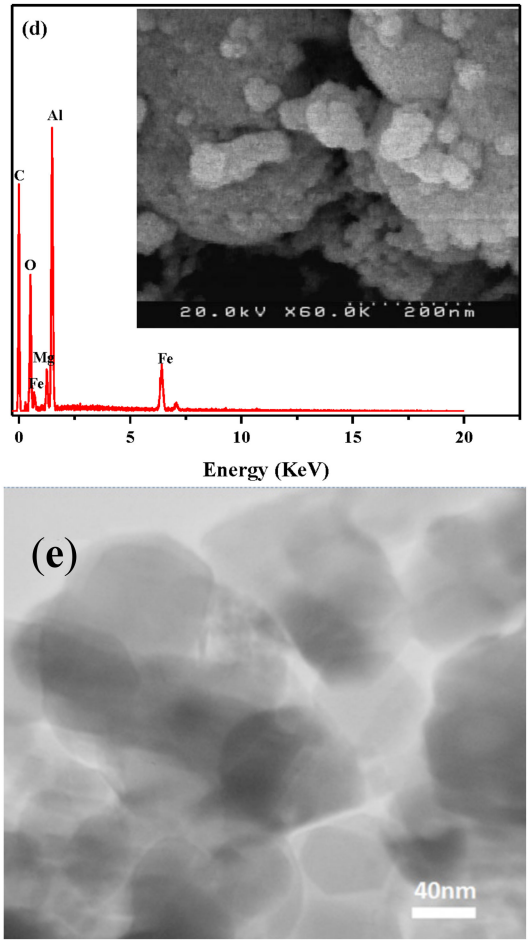

Figure 4. FESEM and EDX of blank Al_2O_3 (**a**); fresh Fe_2O_3-Al_2O_3 (**b**); fresh Fe_2O_3-$MgAl_2O_4$ (**c**); and used Fe_2O_3-$MgAl_2O_4$ (**d**) and TEM of Fe_2O_3-$MgAl_2O_4$ (**e**).

2.2. Activity Results

The catalytic activity of not-modified and modified OC was evaluated in chemical looping CO oxidation, where CO is oxidized to CO_2 in the reduction period and H_2 is produced in the oxidation section. Figure 5 represents the effect of reduction temperature (300–500 °C) on average CO conversion. In addition, the purity of produced hydrogen in the oxidation section at 700 °C for each relevant reduction temperature is shown in this figure. The results show the positive effect of reduction temperature on CO conversion for both samples. For instance, the CO conversion is increased from about 45.3% to 98.3% using the Fe_2O_3-Al_2O_3 oxygen carrier. On the other hand, the conversion of carbon monoxide is 48.2%, 75.7%, 91.3%, 95.2%, and 96.6% at 300, 350, 400, 450, and 500 °C, respectively. The improvement in CO conversion with temperature for both samples is related to the surface activation of iron oxide for oxygen transfer to the reducing agent at elevated temperatures. However, the related H_2 purity in the oxidation section is decreased with a further increase in reduction temperature. In addition to improving the activity of the OC, increasing the reduction temperature facilitates coke formation on its surface. CO disproportionation is an important side reaction that leads to the formation of coke through the following equation [32,33]:

$$2CO \rightarrow C + CO_2. \quad (4)$$

The coke is oxidized in the oxidation section with steam to CO and CO_2 that reduce the purity of produced hydrogen. For example, in the oxidation step related to the reduction temperature of 400 °C,

hydrogen with about 98.5% purity is produced, while oxidation of OC treated in lower reduction temperatures results in the H_2 purity of 100% (Figure 5b). In addition, the CO conversion of about 91.3% is achieved at 400 °C in the reduction period.

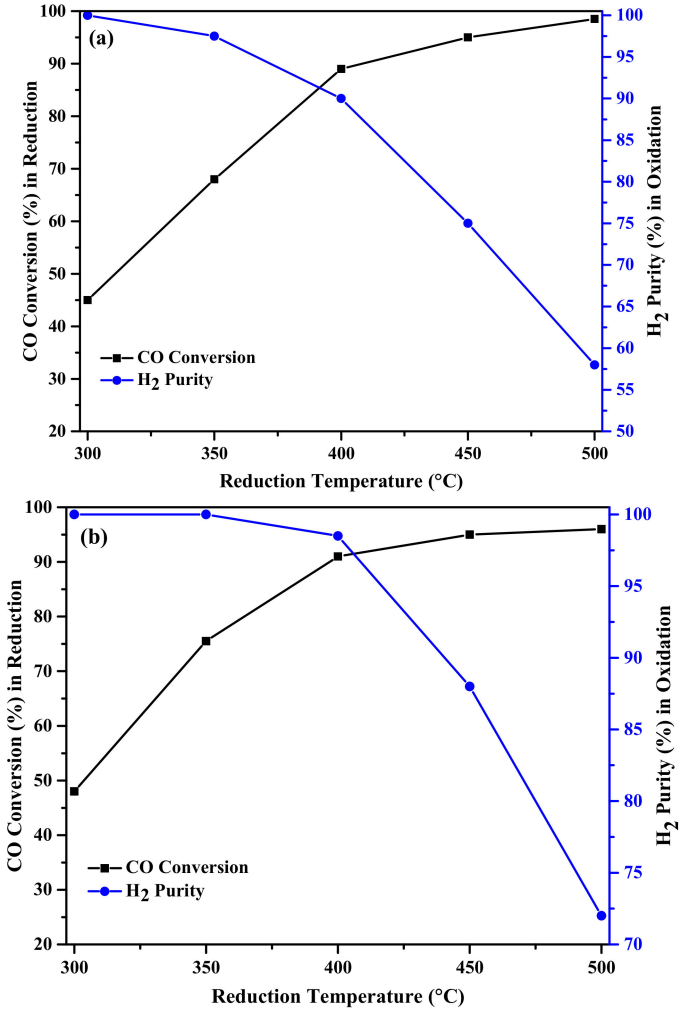

Figure 5. Carbon monoxide conversion at different reduction temperatures and hydrogen purity in the oxidation section using (**a**) the Fe_2O_3-Al_2O_3 oxygen carrier and (**b**) the Fe_2O_3-$MgAl_2O_4$ oxygen carrier.

With the aim of investigating the effect of an Mg promoter on the stability of the synthesized oxygen carriers, the performance of Fe_2O_3-Al_2O_3 and Fe_2O_3-$MgAl_2O_4$ was tested through 20 consecutive reduction-oxidation cycles. Therefore, the variation of CO conversion in the reduction period at 400 °C and the hydrogen purity in the oxidation step over the cycles were determined as shown in Figure 6a,b. The results for the Fe_2O_3-Al_2O_3 oxygen carrier revealed a reduction in CO conversion from 89.9% to 83.5% during 20 redox cycles (about 7%). In addition, the hydrogen purity in the oxidation step is reduced during the cycles (Figure 6a). These behaviors could be mainly due to the deposition of coke on the surface of the oxygen carrier in the reduction step that reduces the purity of produced hydrogen in the oxidation section. However, the crystalline change and destruction in the structure of the oxygen carrier at a high redox temperature has a negative effect on the durability of the sample. On the other hand, the Mg-promoted oxygen carrier (Fe_2O_3-$MgAl_2O_4$) showed a 0.7% reduction in activity through the first five cycles and remained approximately constant over the rest of cycles. The hydrogen purity in the oxidation section is firstly 97.7 and increased to 98.8% in the fifth cycle and remained constant. The improvement in H_2 purity seems to be due to the coke inhibition in

the reduction cycles. This phenomenon is related to the reduction of emitted gases produced from the catalyst's decoking simultaneous with hydrogen production in the reaction between metal and water.

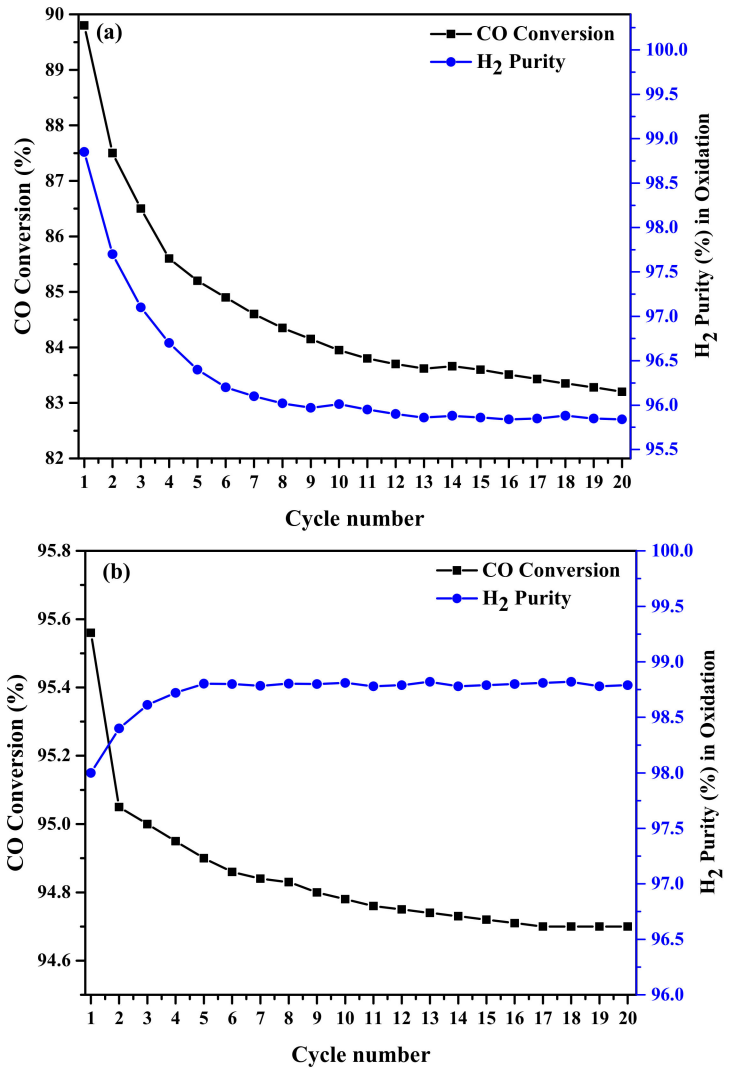

Figure 6. Life time of (**a**) Fe_2O_3-Al_2O_3 and (**b**) Fe_2O_3-$MgAl_2O_4$ oxygen carriers during 20 redox cycles.

In order to better investigate the durability results of the two samples, the CO conversion and hydrogen purity of the first, second, fifth, tenth, and twentieth cycles at 400 °C are demonstrated in Figures 7 and 8. The reduction in CO conversion during each cycle could be related to the reduction in the lattice oxygen of surface active sites with reduction time and coke deposition on the surface. The reduction in CO conversion in the tenth and twentieth cycles compared to the previous cycles shows a continuous reduction in the activity of the oxygen carrier (Figure 7a). On the other hand, the activity of the Mg-promoted sample in Figure 8a revealed that the conversion remained approximately constant after cycle 5. The purity of the produced hydrogen in the oxidation step of both samples increased during the step time to reach 100% (Figures 7 and 8b). The increase in hydrogen purity could be due to the coke decomposition during the process. The higher purity of the produced hydrogen using the Fe_2O_3-$MgAl_2O_4$ oxygen carrier compared to that using the Fe_2O_3-Al_2O_3 oxygen carrier is due to the lower coke deposition.

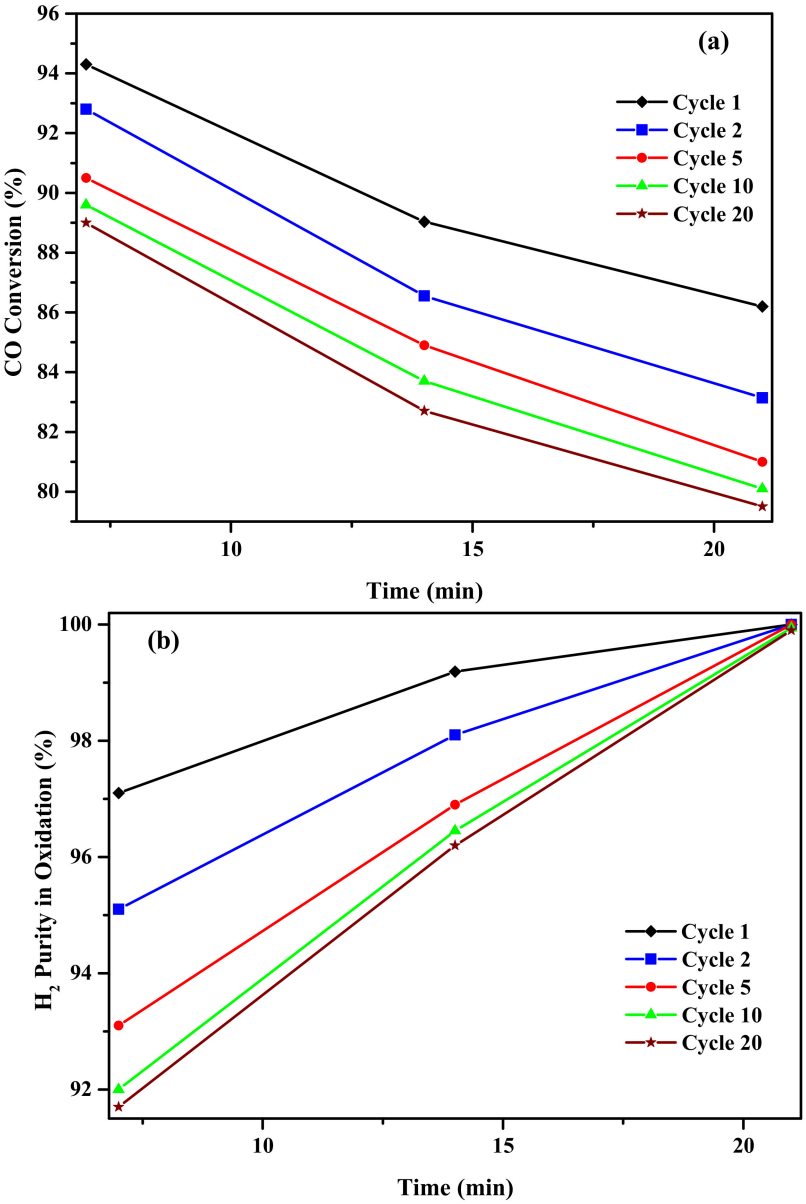

Figure 7. (**a**) The CO conversion and (**b**) hydrogen purity in the oxidation step with time for the Fe_2O_3-Al_2O_3 oxygen carrier at 400 °C (in the reduction step) for different cycles.

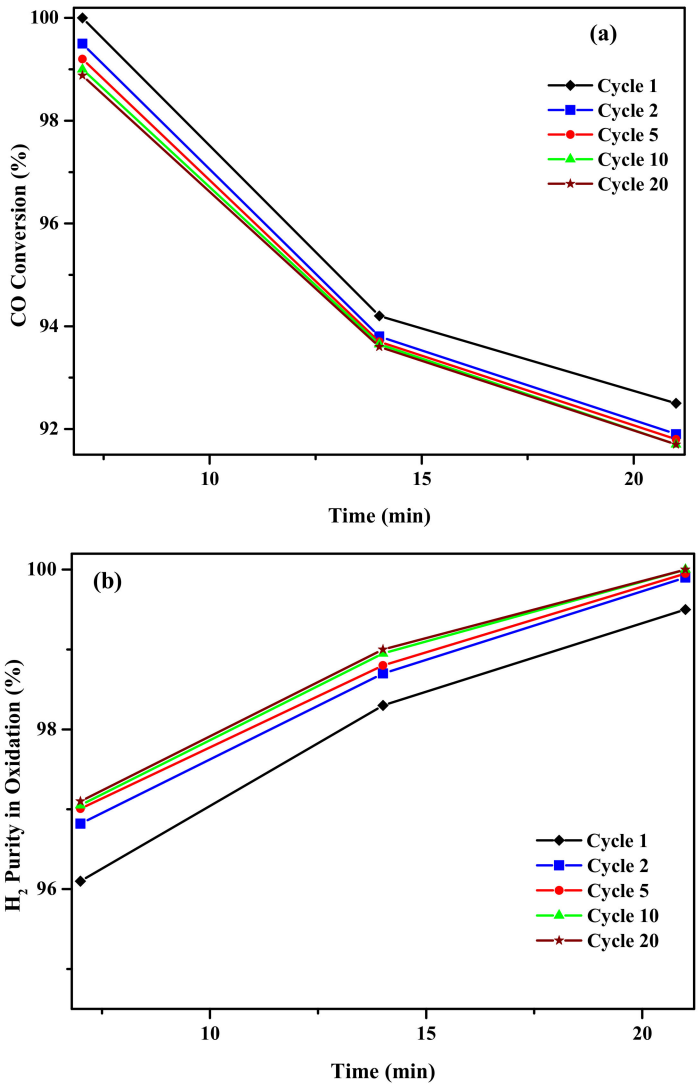

Figure 8. (**a**) The CO conversion and (**b**) hydrogen purity in the oxidation step with time for the Fe_2O_3-$MgAl_2O_4$ oxygen carrier at 400 °C (in the reduction step) for different cycles.

3. Experimental Methods

3.1. Oxygen Carrier Preparation

The OC support affects the performance of oxygen transference, and both alumina and magnesia–alumina spinels were applied as the support for iron oxide. The Fe_2O_3-$MgAl_2O_4$ oxygen transfer material was synthesized using a two-step sequential wetness impregnation method. $MgAl_2O_4$ spinel was prepared by adding a solution of magnesium acetate (0.2 M) to previously synthesized alumina (Al_2O_3 was synthesized by the precipitation method). Prior to impregnation, the slurry was sonicated in a bath-type ultrasound at 30 °C for better incorporation of magnesium precursor into the pores' alumina structure, followed by vacuum impregnation at 80 °C in a rotary evaporator. After that, the sample was dried at 70 °C in a vacuum oven for 10 h. The resulting paste was calcined at 600 °C for 2 h in flowing air. After that, the prepared $MgAl_2O_4$ was used as the support for the preparation of Fe_2O_3-Al_2O_3 or Fe_2O_3-$MgAl_2O_4$ samples. For this purpose, a 0.5 M solution of $Fe(NO_3)_2{\cdot}6H_2O$ (Merck KGaA, Darmstadt, Germany) was added to the as-prepared $MgAl_2O_4$ or Al_2O_3 supports with continuous sonication in a bath ultrasound for 15 min. Subsequently, the impregnated oxygen carrier was dried at 80 °C for 12 h in a vacuum oven followed by calcination at 800 °C for 2 h.

3.2. Oxygen Carrier Characterization

Textual properties, including specific surface area, pore volume, and average pore diameter of the as-prepared samples, were calculated according to the Brunauer–Emmett–Teller (BET) method by N_2 adsorption-desorption isotherms. The specific surface area of the oxygen carriers was measured by BET tests using a (ASAP-2020, Micromeritics, Norcross, GA, USA) gas adsorption apparatus. The Barrett–Joyner–Halenda (BJH) method was implemented to calculate the pore size distributions according to the adsorption branches of the isotherms. The freshly calcined samples were degassed with nitrogen at 200 °C for 3 h prior to the BET test.

The morphology of the synthesized samples was analyzed by an energy dispersive X-ray Spectroscopy (EDX)-equipped field emission scanning electron microscope using a HITACHI S-4160 apparatus (Hitachi, Ltd., Chiyoda, Tokyo, Japan). In addition, a Philips CM30 operated at 300 kV was applied for transmission electron microscopy (TEM) (Philips, Andover, MA, USA). The phase composition and crystallinity of the oxygen transfer materials were analyzed by means of X-ray powder diffraction (XRD; Bruker, D8 Advance, Karlsruhe, Germany) using Cu Kα radiation and operated at 40 kV and 40 mA. The support and oxygen carriers were scanned with 0.05°/s resolution to collect the spectra 2θ between 10° and 90° at ambient temperature.

3.3. Process Activity

In order to evaluate the structural resistance and crystalline transformation of $MgAl_2O_4$-supported Fe_2O_3 as an oxygen carrier, a series of cyclic reduction-oxidation tests were performed at different reduction temperatures (300–500 °C). Hereinafter, the term "cycle" means a reduction cycle involving the reduction of the oxygen carrier with carbon monoxide, followed by oxidation with steam. In the reduction step, carbon monoxide diluted in Ar was fed to the reactor for 21 min and the effluent gas was analyzed continuously. Afterwards, the reduced OC was treated with steam for 21 min in order to reoxidize the sample and hydrogen production simultaneously. Each step in a cycle is dissociated with pure Ar for 20 min in order to drive all of the remaining gases out of the reactor. After 20 reduction-oxidation cycles, the residue oxygen transfer material was examined by the XRD technique.

The activity tests of the chemical looping process were conducted in a fixed-bed reactor with an inner diameter of 16 mm and height of 1000 mm filled with 1 g of finely powdered oxygen carrier with a 100–200 mesh size (Figure 9). The gas streams, including argon (Ar, 100 mL·min^{-1}) as carrier gas and carbon monoxide (CO, 100 mL·min^{-1}) as reactant, were passed through two distinct mass flow controllers (MFC-Unit instruments, model UFC 1661, Yorba Linda, CA, USA) before mixing in the gas mixer. Deionized water was injected into the evaporator with an HPLC pump (Gilson, 307, Middleton, WI, USA) to generate steam. The generated steam was mixed with Ar in a heat-traced pipeline. The products of the reactor were passed through a condenser in order to liquefy the steam and separate them from the gaseous stream. Finally, the products and the unreacted gas streams were analyzed using an online Bruker 450 gas chromatograph (GC-Bruker, 450 series, Billerica, MA, USA) system. The data were collected after one complete cycle in order to ensure the structural stability of the oxygen carriers at a high process temperature.

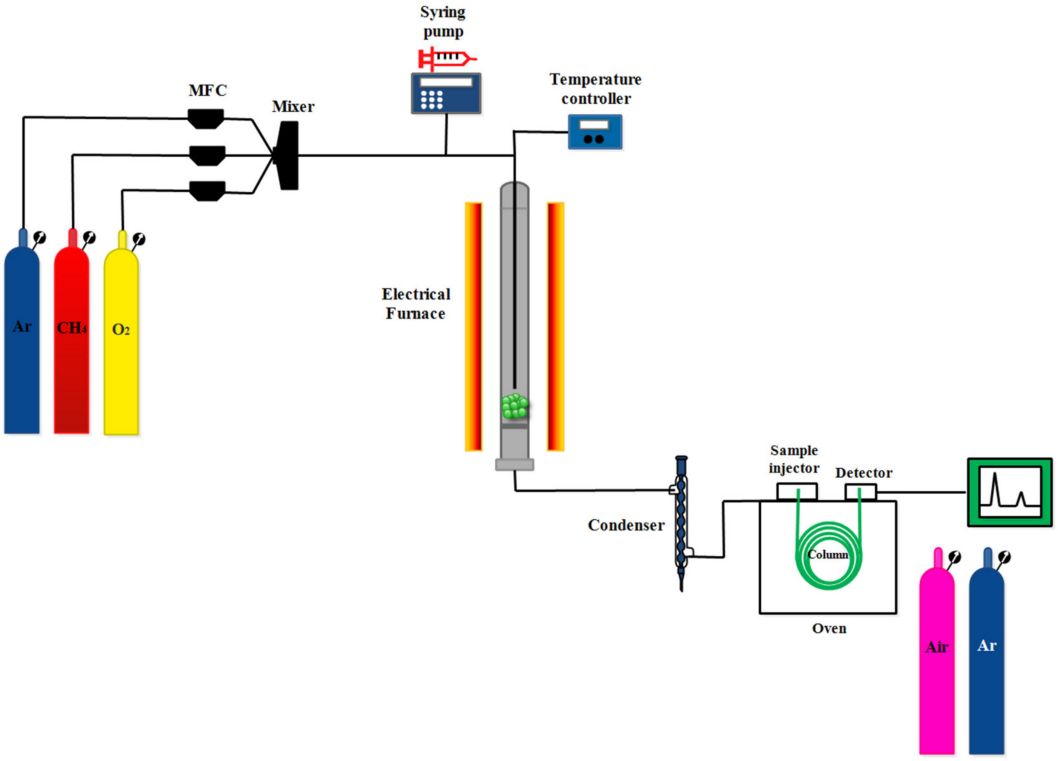

Figure 9. Reactor system for chemical looping hydrogen production.

CO conversion in the reduction section (X_{CO}) was calculated for evaluating the activity of catalyst-sorbents in the chemical looping hydrogen production process according to the following equations.

$$X_{CO} = \frac{(F_{CO_{in}}) - (F_{CO_{out}})}{(F_{CO_{in}})} * 100 \quad (5)$$

where $F_{CO_{in}}$ and $F_{CO_{out}}$ represent the inlet and outlet molar flow rates of carbon monoxide ($mol \cdot min^{-1}$), respectively.

4. Conclusions

In summary, iron oxide was impregnated on a magnesium-modified alumina support for the transference of pure lattice oxygen. The synthesized $MgAl_2O_4$ with a narrow pore size distribution centered at 2.3 nm revealed a better performance on the formation of Fe_2O_3 on the support's surface in comparison with Al_2O_3. However, the higher lattice oxygen transfer capacity could be attained using Fe_2O_3-$MgAl_2O_4$ as an oxygen carrier, which is due to the inhibition of Fe–Al spinel formation. It means that more iron oxides are exposed to transfer lattice oxygen to feed carbon monoxides (for Fe_2O_3-$MgAl_2O_4$ OC) in the fuel reactor compared to Fe_2O_3-Al_2O_3 with more iron atoms associated in spinel of Fe–Al. In addition, the characterization results of the Fe_2O_3-$MgAl_2O_4$ sample showed the agglomeration of particles with a diameter of about 40–50 nm. The modified OC was applied in chemical looping CO oxidation cycles. The obtained results revealed that increasing the reduction temperature to higher than 400 °C accelerates coke formation on the OC's surface. The conversion of deposited coke in the oxidation section reduced the purity of produced hydrogen in the oxidation section. A CO conversion of 91.3% and hydrogen purity of about 98.5% were achieved in the reduction (400 °C) and oxidation periods, respectively.

Author Contributions: A.H. conceived and designed the experiments, performed the experiments, performed the catalyst synthesis, and analyzed the data; M.R.R. contributed reagents/materials/analysis tools and participated in the analysis and interpretation of the characterization results; and A.H. and M.R.R. wrote the paper.

Conflicts of Interest: The authors declare no conflict of interest.

References

1. Sarshar, Z.; Kleitz, F.; Kaliaguine, S. Novel oxygen carriers for chemical looping combustion: $La_{1-x}CexBO_3$ (B = Co, Mn) perovskites synthesized by reactive grinding and nanocasting. *Energy Environ. Sci.* **2012**, *4*, 4258–4269. [CrossRef]
2. Hafizi, A.; Rahimpour, M.R.; Hassanajili, S. Hydrogen production via chemical looping steam methane reforming process: Effect of cerium and calcium promoters on the performance of Fe_2O_3/Al_2O_3 oxygen carrier. *Appl. Energy* **2016**, *165*, 685–694. [CrossRef]
3. Mohsenzadeh, A.; Richards, T.; Bolton, K. DFT study of the water gas shift reaction on Ni(111), Ni(100) and Ni(110) surfaces. *Surf. Sci.* **2016**, *644*, 53–63. [CrossRef]
4. Tang, Q.-L.; Chen, Z.-X.; He, X. A theoretical study of the water gas shift reaction mechanism on Cu(111) model system. *Surf. Sci.* **2009**, *603*, 2138–2144. [CrossRef]
5. Alihoseinzadeh, A.; Khodadadi, A.A.; Mortazavi, Y. Enhanced catalytic performance of Au/CuO–ZnO catalysts containing low CuO content for preferential oxidation of carbon monoxide in hydrogen-rich streams for PEMFC. *Int. J. Hydrogen Energy* **2014**, *39*, 2056–2066. [CrossRef]
6. Tosti, S.; Zerbo, M.; Basile, A.; Calabrò, V.; Borgognoni, F.; Santucci, A. Pd-based membrane reactors for producing ultra-pure hydrogen: Oxidative reforming of bio-ethanol. *Int. J. Hydrogen Energy* **2013**, *38*, 701–707. [CrossRef]
7. Akbari-Emadabadi, S.; Rahimpour, M.R.; Hafizi, A.; Keshavarz, P. Promotion of Ca-Co bifunctional catalyst/sorbent with yttrium for hydrogen production in modified chemical looping steam methane reforming. *Catalysts* **2017**, *7*, 270. [CrossRef]
8. Liu, W.; Ismail, M.; Dunstan, M.T.; Hu, W.; Zhang, Z. Fennell PS Inhibiting the interaction between FeO and Al_2O_3 during chemical looping production of hydrogen. *RSC Adv.* **2015**, *5*, 1759–1771. [CrossRef]
9. Akbari-Emadabadi, S.; Rahimpour, M.R.; Hafizi, A.; Keshavarz, P. Production of hydrogen-rich syngas using Zr modified Ca-Co bifunctional catalyst-sorbent in chemical looping steam methane reforming. *Appl. Energy* **2017**, *206*, 51–62. [CrossRef]
10. Alirezaei, I.; Hafizi, A.; Rahimpour, M.R. Syngas production in chemical looping reforming process over ZrO_2 promoted Mn-based catalyst. *J. CO_2 Util.* **2017**, *23*, 105–116. [CrossRef]
11. Hafizi, A.; Rahimpour, M.R.; Hassanajili, S. Calcium promoted Fe/Al_2O_3 oxygen carrier for hydrogen production via cyclic chemical looping steam methane reforming process. *Int. J. Hydrogen Energy* **2015**, *40*, 16159–16168. [CrossRef]
12. Zhu, X.; Sun, L.; Zheng, Y.; Wang, H.; Wei, Y.; Li, K. CeO_2 modified Fe_2O_3 for the chemical hydrogen storage and production via cyclic water splitting. *Int. J. Hydrogen Energy* **2014**, *39*, 13381–13388. [CrossRef]
13. Alirezaei, I.; Hafizi, A.; Rahimpour, M.R.; Raeissi, S. Application of zirconium modified Cu-based oxygen carrier in chemical looping reforming. *J. CO_2 Util.* **2016**, *14*, 112–121. [CrossRef]
14. Ortiz, M.; de Diego, L.F.; Abad, A.; García-Labiano, F.; Gayán, P.; Adánez, J. Catalytic Activity of Ni-Based Oxygen-Carriers for Steam Methane Reforming in Chemical-Looping Processes. *Energy Fuels* **2012**, *26*, 791–800. [CrossRef]
15. Forutan, H.; Karimi, E.; Hafizi, A.; Rahimpour, M.R.; Keshavarz, P. Expert representation chemical looping reforming: A comparative study of Fe, Mn, Co and Cu as oxygen carriers supported on Al_2O_3. *J. Ind. Eng. Chem.* **2015**, *21*, 900–911. [CrossRef]
16. Hacker, V.; Faleschini, G.; Fuchs, H.; Fankhauser, R.; Simader, G.; Ghaemi, M.; Spreitz, B.; Friedrich, M. Usage of biomass gas for fuel cells by the SIR process. *J. Power Sources* **1998**, *71*, 226–230. [CrossRef]
17. Hacker, V.; Fankhauser, R.; Faleschini, G.; Fuchs, H.; Friedrich, K.; Muhr, M.; Kordesch, K. Hydrogen production by steam–iron process. *J. Power Sources* **2000**, *86*, 531–535. [CrossRef]
18. Hafizi, A.; Rahimpour, M.R.; Hassanajili, S. High purity hydrogen production via sorption enhanced chemical looping reforming: Application of $22Fe_2O_3/MgAl_2O_4$ and $22Fe_2O_3/Al_2O_3$ as oxygen carriers and cerium promoted CaO as CO_2 sorbent. *Appl. Energy* **2016**, *169*, 629–641. [CrossRef]

19. Li, F.; Sun, Z.; Luo, S.; Fan, L.S. Ionic diffusion in the oxidation of iron—Effect of support and its implications to chemical looping applications. *Energy Environ. Sci.* **2011**, *4*, 876–880. [CrossRef]
20. Xu, B.-Q.; Wei, J.-M.; Wang, H.-Y.; Sun, K.-Q.; Zhu, Q.-M. Nano-MgO: Novel preparation and application as support of Ni catalyst for CO_2 reforming of methane. *Catal. Today* **2001**, *68*, 217–225. [CrossRef]
21. Kambolis, A.; Matralis, H.; Trovarelli, A.; Papadopoulou, C. Ni/CeO_2-ZrO_2 catalysts for the dry reforming of methane. *Appl. Catal. A Gen.* **2010**, *377*, 16–26. [CrossRef]
22. Hafizi, A.; Rahimpour, M.R.; Hassanajili, S. Hydrogen production by chemical looping steam reforming of methane over Mg promoted iron oxygen carrier: Optimization using design of experiments. *J. Taiwan Inst. Chem. Eng.* **2016**, *62*, 140–149. [CrossRef]
23. Rezaei, M.; Alavi, S.; Sahebdelfar, S.; Bai, P.; Liu, X.; Yan, Z.-F. CO_2 reforming of CH_4 over nanocrystalline zirconia-supported nickel catalysts. *Appl. Catal. B Environ.* **2008**, *77*, 346–354. [CrossRef]
24. Wang, N.; Yu, X.; Shen, K.; Chu, W.; Qian, W. Synthesis, characterization and catalytic performance of MgO-coated Ni/SBA-15 catalysts for methane dry reforming to syngas and hydrogen. *Int. J. Hydrogen Energy* **2013**, *38*, 9718–9731. [CrossRef]
25. Laosiripojana, N.; Sutthisripok, W.; Assabumrungrat, S. Synthesis gas production from dry reforming of methane over CeO_2 doped Ni/Al_2O_3: Influence of the doping ceria on the resistance toward carbon formation. *Chem. Eng. J.* **2005**, *112*, 13–22. [CrossRef]
26. Huang, L.; Xie, J.; Chen, R.; Chu, D.; Chu, W.; Hsu, A.T. Effect of iron on durability of nickel-based catalysts in auto-thermal reforming of ethanol for hydrogen production. *Int. J. Hydrogen Energy* **2008**, *33*, 7448–7456. [CrossRef]
27. Hafizi, A.; Jafari, M.; Rahimpour, M.R.; Hassanajili, S. Experimental investigation of sorption enhanced chemical looping reforming for high purity hydrogen production using CeO_2–CaO CO_2 sorbent and 15Fe–5Ca/Al_2O_3 oxygen carrier. *J. Taiwan Inst. Chem. Eng.* **2016**, *65*, 185–196. [CrossRef]
28. Li, D.; Zeng, L.; Li, X.; Wang, X.; Ma, H.; Assabumrungrat, S.; Gong, J. Ceria-promoted Ni/SBA-15 catalysts for ethanol steam reforming with enhanced activity and resistance to deactivation. *Appl. Catal. B Environ.* **2015**, *176*, 532–541. [CrossRef]
29. Jabbour, K.; Massiani, P.; Davidson, A.; Casale, S.; Hassan, N. Ordered mesoporous "one-pot" synthesized Ni-Mg(Ca)-Al_2O_3 as effective and remarkably stable catalysts for combined steam and dry reforming of methane (CSDRM). *Appl. Catal. B Environ.* **2017**, *201*, 527–542. [CrossRef]
30. Jiang, B.; Dou, B.; Wang, K.; Song, Y.; Chen, H.; Zhang, C.; Xu, Y.; Li, M. Hydrogen production from chemical looping steam reforming of glycerol by Ni based Al-MCM-41 oxygen carriers in a fixed-bed reactor. *Fuel* **2016**, *183*, 170–176. [CrossRef]
31. Ren, B.; Zhang, L.; Tang, C.; Dong, L.; Li, J. Construction of hierarchical $MgAl_2O_4$ spinel as catalytic supports. *Mater. Lett.* **2015**, *159*, 204–206. [CrossRef]
32. Damyanova, S.; Pawelec, B.; Arishtirova, K.; Fierro, J. Ni-based catalysts for reforming of methane with CO_2. *Int. J. Hydrogen Energy* **2012**, *37*, 15966–15975. [CrossRef]
33. Wang, P.; Tanabe, E.; Ito, K.; Jia, J.; Morioka, H.; Shishido, T.; Takehira, K. Filamentous carbon prepared by the catalytic pyrolysis of CH_4 on Ni/SiO_2. *Appl. Catal. A Gen.* **2002**, *231*, 35–44. [CrossRef]